Inorganic Chemistry

Article

pubs.acs.org/IC

Structural Design Parameters for Highly Birefringent Coordination Polymers

John R. Thompson,[†,‡] Michael J. Katz,[†,§] Vance E. Williams,*[,†,‡] and Daniel B. Leznoff*[,†]

[†]Department of Chemistry, Simon Fraser University, 8888 University Drive, Burnaby, British Columbia V5A 1S6, Canada

[‡]4D LABORATORIES, Simon Fraser University, 8888 University Drive, Burnaby, British Columbia V5A 1S6, Canada

Supporting Information

ABSTRACT: A series of coordination polymer materials incorporating the highly anisotropic 2-(2-pyridyl)-1,10-phenanthroline (phenpy) building block have been synthesized and structurally characterized. $M(phenpy)[Au(CN)_2]_2$ (M = Cd, Mn) are isostructural and form a 1-D chain through bridging $[Au(CN)_2]^-$ units and extend into a 2-D sheet through aurophilic interactions. $M(phenpy)(H_2O)[Au(CN)_2]_2\cdot 2H_2O$ (M = Cd, Mn, and Zn) are also isostructural but differ from the first set via the inclusion of a water molecule into the coordination sphere, resulting in a 1-D topology through aurophilic interactions. $In(phenpy)(Cl)_2[Au(CN)_2]\cdot 0.5H_2O$ forms a dimer through bridging chlorides and contains a free $[Au(CN)_2]^-$ unit. In the plane of the primary crystal growth direction, the birefringence values (Δn) of 0.37(2) ($Cd(phenpy)[Au(CN)_2]_2$), 0.50(3) ($In(phenpy)(Cl)_2[Au(CN)_2]\cdot 0.5H_2O$), 0.56(3) and 0.59(6) ($M(phenpy)(H_2O)[Au(CN)_2]_2\cdot 2H_2O$ M = Cd and Zn, respectively) were determined. β, a structural parameter defined by phenpy units rotated in the $A-C$ plane relative to the light propagation (C) direction, was found to correlate to Δn magnitudes. The addition of a carbon−carbon double bond to terpy has increased the molecular polarizability anisotropy of the building block, and all structures have reduced deviation from planarity in comparison to terpy and terpy derivative structures, leading to these higher Δn values, which are among the highest reported for crystalline solids.

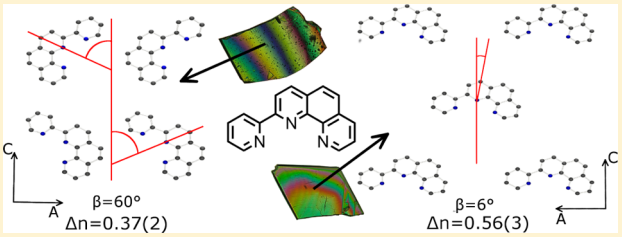

INTRODUCTION

Birefringence (Δn) arises when the refractive index (n) depends on the direction of light propagation through a medium; it is therefore a fundamental property of anisotropic materials.[1−3] Birefringent crystals are used as optical filters,[4−8] as quarter-wave plates for generating circularly polarized light,[1−3] and in NLO phase matching.[9−13] According to the Lorentz−Lorenz equation, the refractive index is determined by both the density and polarizability of a material; birefringence is the manifestation of the orientation-dependent differences in the two quantities.[1−3] If light traveling through a material interacts with a greater number of atoms and/or more highly polarizable atoms in one direction, its propagation will be slower along that path.[14] As such, birefringence can be tuned by tailoring a material's polarizability and density anisotropies in order to maximize the differences in light retardation along different vectors.

Previously, we have identified several criteria for designing highly birefringent crystalline materials.[15] Ideally, the following will apply: (1) a material should be constructed from building blocks with high polarizability anisotropies; (2) the building blocks should be oriented with a parallel alignment to one another; (3) the crystals must be of sufficient optical quality; and (4) the crystals must have a favorable crystal growth direction. Whereas criteria 1 and 2 control the absolute birefringence of a crystal, criteria 3 and 4 determine the magnitude of the birefringence that can actually be measured and exploited. Poor quality crystals, or those that fail to present an appropriate crystal face to the observer, will exhibit less than optimum optical properties.

We have shown that the alignment of anisotropic building blocks can be achieved through their incorporation into coordination polymers, which can result in highly birefringent materials.[15−18] For example, 2,2′;6′2″-terpyridine (terpy) crystallizes in a herringbone structure[19,20] that leads to a partial cancellation of the supramolecular anisotropy; hence, these crystals have a low anisotropy. In contrast, coordination polymers in which the terpy ligands are aligned parallel to each other result in materials with observed birefringence values (Δn) of up to 0.43(4).[16] In comparison, calcite, the commercial standard, has $\Delta n = 0.172$;[2] quartz has a low birefringence of $\Delta n = 0.009$.[1,2,21] Calomel (Hg_2Cl_2) is an example of a highly birefringent inorganic solid, with $\Delta n = 0.683$.[21]

Following the criteria outlined above, increasing the polarizability anisotropy of the terpy ligand is expected to afford more highly birefringent materials. We previously reported the effect of placing highly polarizable halo substituents at the 4′ position of the terpy;[17] this strategy met with mixed results. Although Δn values as high as 0.50(3) were observed, these halo-terpy ligands tended to give less predictable results. Since addition of the halo moieties gave rise

Received: April 4, 2015
Published: June 22, 2015

DOI: 10.1021/acs.inorgchem.5b00749
Inorg. Chem. 2015, 54, 6462−6471

to structures in which the terpy groups were less planar (contrary to criteria 2) and in which the highly polarizable C-halo bond aligned along the crystal growth direction, where it cannot contribute meaningfully to the measurable birefringence (contrary to criteria 4), the observed Δn values for a range of halo-terpy-containing coordination polymers were as low as 0.26(3).

In light of these issues, and in particular the tendency of the terpy derivatives to deplanarize (we have observed torsion angles of 6.5−20.5° between pyridine planes in a range of coordination polymers),[16,17] we targeted a new ligand, 2-(2-pyridyl)-1,10-phenanthroline (phenpy),[22] in which the tridentate pyridine donor motif is preserved but one double bond is added to the backbone, connecting two of the pyridine rings together (Figure 1). This design feature adds further

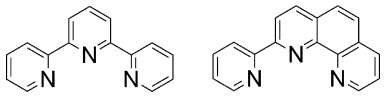

Figure 1. Comparison of terpy (left) and phenpy ligands.

constraints on the ligand, and restricting the degrees of freedom should lead to more planar systems and a more reliable building block in terms of maximizing structural anisotropy. The placement of the double bond in the ring also increases the polarizability anisotropy of the ligand framework by adding more polarizability in the plane of the ligand by extending the π -system,[14] while maintaining the same overall shape and color as terpy. Thus, since phenpy is a close structural analogue to terpy, it should give structures with similar coordination environments to terpy and other terpy analogues.

To this end, we targeted the synthesis of materials incorporating phenpy units aligned using (nearly) colorless manganese(II), zinc(II), cadmium(II), and indium(III) metal centers with $[Au(CN)_2]^-$ or halide bridging units as a comparison with prior terpy-based materials, and their structures and birefringent properties were investigated in light of these design principles.

RESULTS AND DISCUSSION

Structure of M(phenpy)[Au(CN)$_2$]$_2$ (M = Mn and Cd). The hydrothermal synthesis reaction of manganese(II) or cadmium(II) salts with phenpy and 2 equiv of $[Au(CN)_2]^-$ results in the formation of crystals of isomorphous M(phenpy)-$[Au(CN)_2]_2$ (M = Mn and Cd). As a representative example, the structure of Mn(phenpy)$[Au(CN)_2]_2$ is described; it

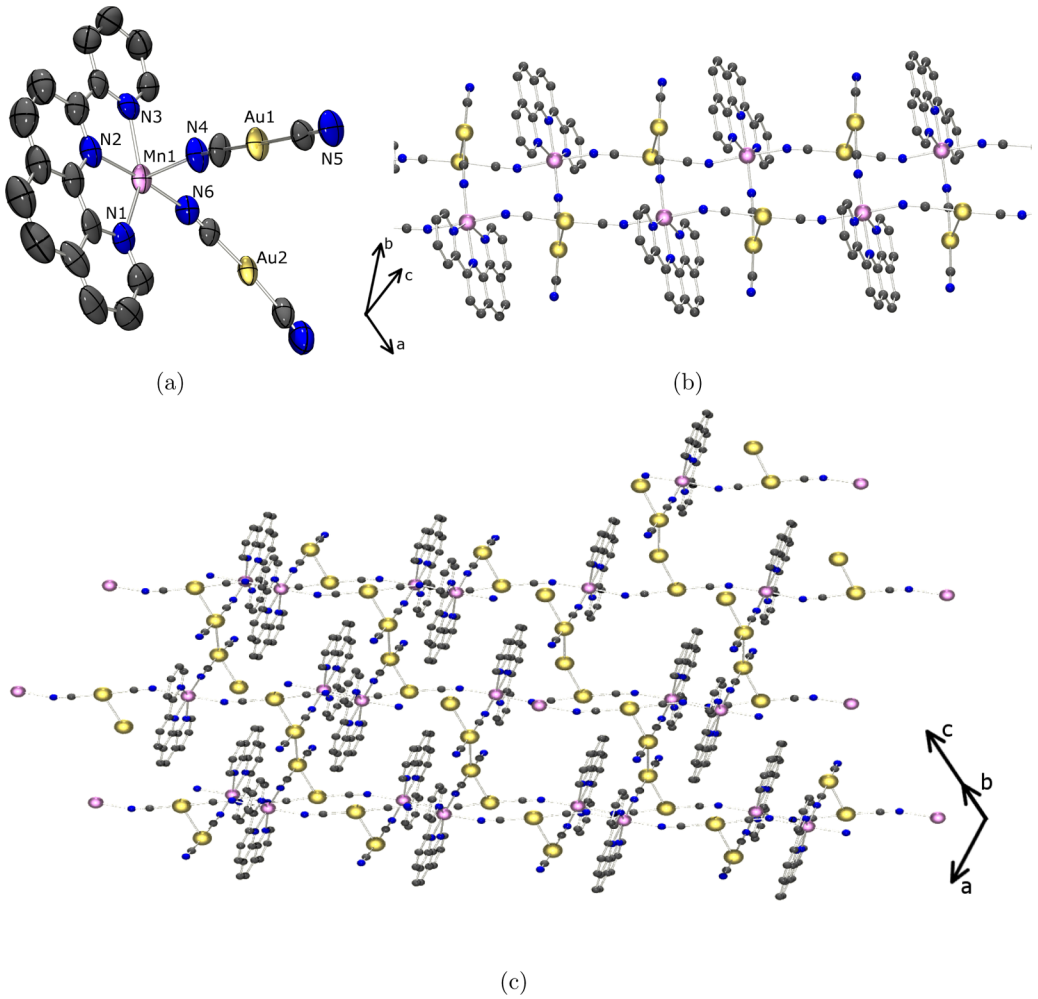

Figure 2. Crystal structure of Mn(phenpy)$[Au(CN)_2]_2$: (a) local geometry showing thermal ellipsoids; (b) 1-D chain of Mn(phenpy)$[Au(CN)_2]_2$ showing all the phenpy molecules aligned face-to-face; (c) 2-D sheet of Mn(phenpy)$[Au(CN)_2]_2$ showing tetramers of $[Au(CN)_2]^-$ units. Atom colors: orchid, Mn; gold, Au; blue, N; gray, C.

DOI: 10.1021/acs.inorgchem.5b00749
Inorg. Chem. 2015, 54, 6462−6471

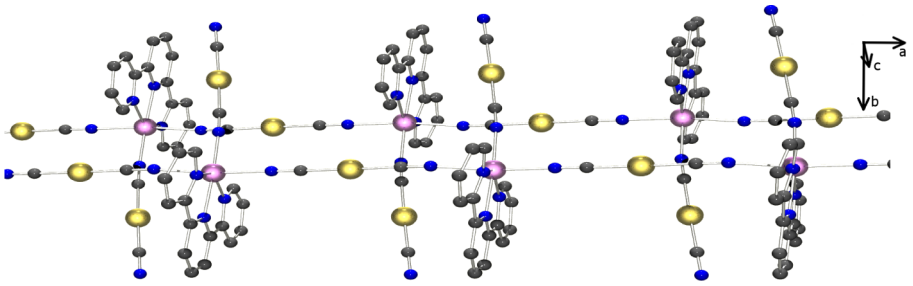

Figure 3. Crystal structure of Mn(terpy)$[Au(CN)_2]_2$ and its 1-D ladder topology.[16] Atom colors: orchid, Mn; gold, Au; blue, N; gray, C.

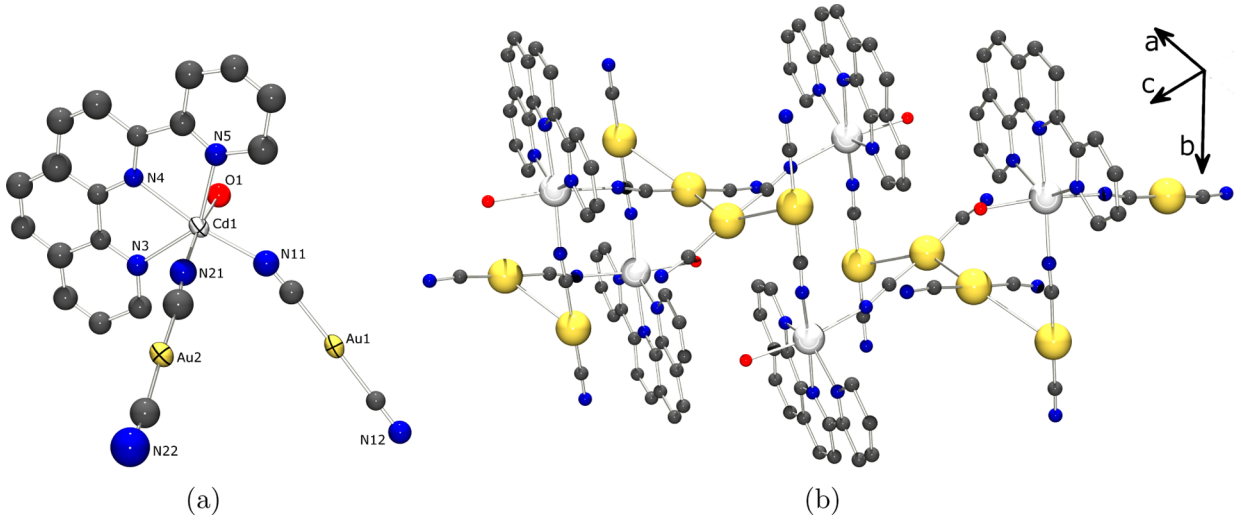

Figure 4. Crystal structure of Cd(phenpy)$(H_2O)[Au(CN)_2]_2\cdot 2H_2O$: (a) local geometry showing thermal ellipsoids; (b) 1-D chain of Cd(phenpy)$(H_2O)[Au(CN)_2]_2\cdot 2H_2O$ showing all the phenpy molecules aligned face-to-face. Atom colors: silver, Cd; gold, Au; red, O; blue, N; gray, C.

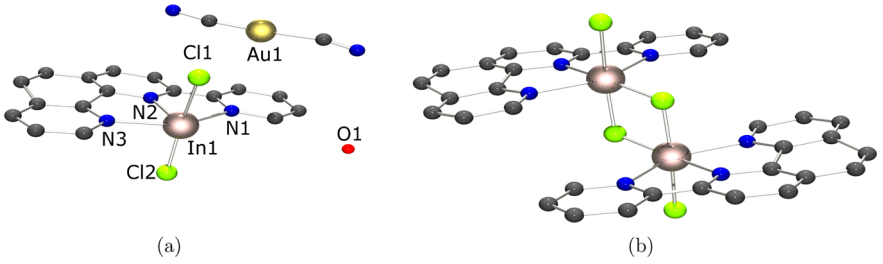

Figure 5. Crystal structure of In(phenpy)$(Cl)_2[Au(CN)_2]\cdot 0.5H_2O$ (a) local geometry. (b) A dimer of In(phenpy)$(Cl)_2[Au(CN)_2]\cdot 0.5H_2O$ showing the phenpy molecules aligned face-to-face. Only one of the two disordered phenpy ligands is shown for clarity. Atom colors: pink, In; gold, Au; green, Cl; red, O; blue, N; gray, C.

contains a Mn(II) center with an octahedral coordination environment (Figure 2a) consisting of one phenpy (Mn−N = 2.30(2), 2.21(2), and 2.29(1) Å), and two bridging and one terminal $[Au(CN)_2]^-$ units (Mn−N = 2.21(1), 2.22(1), 2.12(2) Å). The phenpy ligand deviates from planarity by a torsion angle of 3.6°, which is significantly less than that of the analogous terpy-containing species.[16,17]

The extended structure (Figure 2b) is built via bridging $[Au(CN)_2]^-$ units forming a 1-D chain. Aurophilic interactions of 3.060(1) Å between terminal $[Au(CN)_2]^-$ units create a 1-D ladder. Further aurophilic interactions of 3.252 Å create a tetramer of $[Au(CN)_2]^-$ units, which generate a 2-D sheet (Figure 2c).

Mn(phenpy)$[Au(CN)_2]_2$ is isostructural with that of the previously published Mn(4′-Brterpy)$[Au(CN)_2]_2$.[17] It is also similar to Mn(terpy)$[Au(CN)_2]_2$ (Figure 3) in that both form 1-D ladder structures; however, Mn(phenpy)$[Au(CN)_2]_2$ has an extra aurophilic interaction that creates the aforementioned $[Au(CN)_2]^-$ tetramers.[16]

Structure of M(phenpy)$(H_2O)[Au(CN)_2]_2\cdot 2H_2O$ (M = Mn, Zn, and Cd). The reaction of manganese(II), zinc(II), or cadmium(II) salts with phenpy and 2 equiv of $[Au(CN)_2]^-$ via slow evaporation of a water/methanol solution (instead of under hydrothermal conditions as above) produced isomorphous crystals of M(phenpy)$(H_2O)[Au(CN)_2]_2\cdot 2H_2O$ (M = Mn, Zn, and Cd). As a representative example, the structure of Cd(phenpy)$(H_2O)[Au(CN)_2]_2\cdot 2H_2O$ contains an octahedral metal center (Figure 4a), with one phenpy molecule (Cd−N = 2.38(2) and 2.32(2) Å, torsion angle 2.0°), two terminal $[Au(CN)_2]^-$ units (Cd−N = 2.23(2) and 2.31(2) Å), and a

DOI: 10.1021/acs.inorgchem.5b00749
Inorg. Chem. 2015, 54, 6462−6471

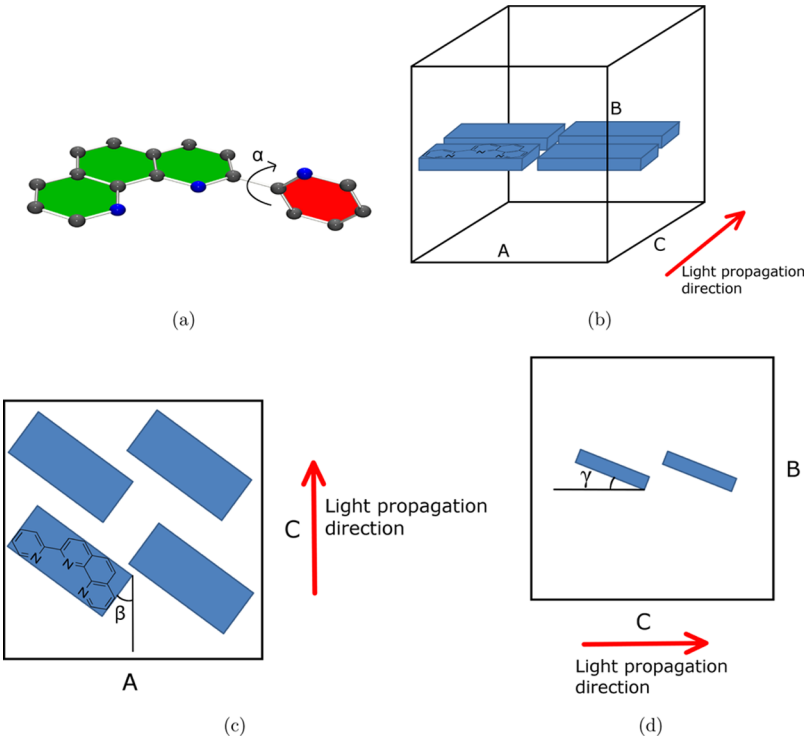

Figure 6. Angles discussed in the birefringence analysis: (a) the torsion angle (α) within each phenpy molecule, defined as the angle between the green and red planes. (b) A general depiction of the relative orientation of phenpy molecules (blue blocks) to the direction of light propagation (C). (c) The angle (β) between the direction of light propagation and phenpy units rotated in the $A-C$ plane. (d) The angle (γ) between the direction of light propagation and phenpy units rotated in the $B-C$ plane. Atom colors: blue, N; gray, C.

bound water molecule (Cd−O = 2.35(1) Å). There are also two interstitial water molecules in the crystal. Aurophilic interactions of 3.277(3) and 3.460(2) Å link the molecules to one another, forming a 1-D chain (Figure 4b).

Although this different synthetic procedure yields a different structure (Figure 4b vs Figure 3), with the bound H_2O unit blocking the binding of bridging $[Au(CN)_2]^-$ units, the material still shows a high alignment of the phenpy units as required for high birefringence (criteria 2).

Structure of In(phenpy)(Cl)$_2$[Au(CN)$_2$]·0.5H$_2$O. Switching from M^{2+} cations to the M^{3+} containing $InCl_3 \cdot 3H_2O$ results in a very different structure. The reaction with phenpy and 3 equiv of $[Au(CN)_2]^-$ via slow evaporation of a water/methanol solution produced crystals of $In(phenpy)(Cl)_2[Au(CN)_2] \cdot 0.5H_2O$. The structure contains an octahedral In^{3+} center (Figure 5), with one phenpy ligand (torsion angle ≈ 3.5°) and two axial and one equatorial chloride ligands. The chloride in the equatorial plane changes to the axial position of a neighboring In center, creating a dimer (Figure 5). The structure shows good stacking of the phenpy units; in addition, the $[Au(CN)_2]^-$ unit aligns in a parallel fashion with the phenpy ligand, adding to the overall polarizability anisotropy of the system.

Structure−Birefringence analysis. In order to facilitate the comparison of crystal structures that are not isostructural in the rationalization of the differences in birefringence values and develop meaningful conclusions, each structure will be simplified. The source of the majority of the polarizability anisotropy in the overall structure is likely from the phenpy units;[14,16,23] therefore, each structure will be assessed by examining only the planarity of the phenpy units and the relative orientation of the phenpy units with respect to the light propagation direction. To facilitate this structure−property analysis three angles have been identified (Figure 6) and are defined as the torsion angle (α) within each phenpy molecule (Figure 6a): the angle (β) between the direction of light propagation and phenpy units rotated in the $A-C$ plane (Figure 6c), and the angle (γ) between the direction of light propagation and phenpy units rotated in the $B-C$ plane (Figure 6d), where A, B, and C are denoted in Figure 6b. In order to assess the importance of these angles with respect to the birefringence, the polarizability tensor for phenpy was calculated.

Figure 7 shows a phenpy molecule with axes labeled depicting the result of a polarizability calculation (DFT B3LYP 6-31G**) based on the phenpy nuclear coordinates taken from the crystal structure of $Cd(phenpy)(H_2O)[Au(CN)_2]_2 \cdot 2H_2O$. The polarizability tensor components have

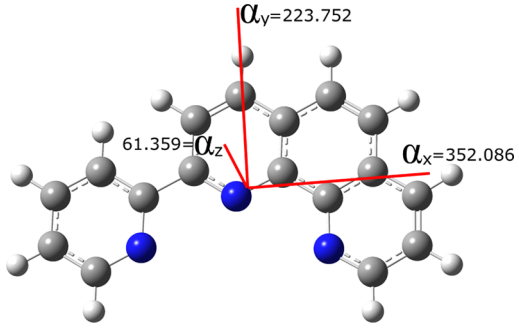

Figure 7. Phenpy molecule labeled with the polarizability tensor axes and the calculated polarizabilities α_x, α_y, and α_z. Atom colors: blue, N; gray, C; white, H.

DOI: 10.1021/acs.inorgchem.5b00749
Inorg. Chem. 2015, 54, 6462−6471

values of 352.086, 223.752, and 61.359 au (1 au = 1.649 × 10^{-41} C^2 m^2 J^{-1}) for α_x, α_y, and α_z, respectively. The lowest polarizability is the α_z tensor component, which is perpendicular to the plane of the phenpy unit, and the largest is the α_x tensor component, which is parallel to the longest phenpy dimension. Therefore, the ideal orientation of phenpy units in a crystal in order to maximize the polarizability anisotropy and thereby the birefringence would be the case where the light propagation is parallel to the α_y-axis, so that the resulting measure of birefringence is based on the difference between the α_x and α_z tensor components of phenpy.

In order to achieve this maximum possible polarizability anisotropy of the crystal, angles α, β, and γ should all equal zero. When nonzero, these angles all decrease the polarizability anisotropy contribution of the phenpy unit. However, the Δn value is expected to be most sensitive to γ, which leads to averaging of two very disparate polarizability tensor components (α_y and α_z). Any nonzero value of γ will increase the polarizability in the B direction (Figure 6b) as it will lead to some α_y component in this direction, thus decreasing the polarizability anisotropy experienced by light propagating in the C direction.

In addition, crystals with large β values will also experience a significant decrease in the polarizability anisotropy because the polarizability tensor component α_y is approximately two-thirds of α_x. Therefore, increasing β results in the polarizability in the A direction containing some α_y component, leading to the overall anisotropy being the difference between α_z and weighted average $\alpha_x - \alpha_y$ and consequently a reduced birefringence.

With this toolbox for supramolecular structure−property analysis in place, birefringence measurements for the three structure types described above, and a case by case examination of the structural features leading to the observed Δn, are described below.

Birefringence. The birefringence values of all compounds were obtained using the Berek method at λ = 546(10) nm at room temperature. Retardation measurements were also conducted at λ = 650(20) nm, resulting in a <1% difference compared to the measurements at 546 nm, indicating that the birefringence is not wavelength dependent in this region. Consistent with this observation, solution UV−vis data for Phenpy, $Zn(phenpy)(NO_3)_2$, $Mn(phenpy)Cl_2$, and $Cd(phenpy)(NO_3)_2$ showed no absorption above 400 nm, indicating that the birefringence values are not resonance-enhanced (Figure S1). Measurements for all compounds were made parallel to the [010]-axis.

Birefringence of M(phenpy)[Au(CN)$_2$]$_2$ (M = Mn and Cd). The measured birefringence of $Cd(phenpy)[Au(CN)_2]_2$ is 0.37(2). No measurement of $Mn(phenpy)[Au(CN)_2]_2$ could be made due to poor crystal quality. The crystals of $M(phenpy)[Au(CN)_2]_2$ have plate morphology and are monoclinic, growing perpendicular to the b-axis. Since the b-axis contains a symmetry element, one of the three components of the indicatrix is aligned along this axis. Therefore, the measured birefringence represents the difference between the remaining two primary components of the indicatrix (n_{ac1} and n_{ac2}). A view down the b-axis (Figure 8a) shows good alignment of phenpy units; however, there is a slight tilt in the phenpy units with respect to the light propagation as reflected in a γ angle (Figure 6c) of 4.0° and therefore a small cancellation of the polarizability anisotropy. The α torsion angle is 3.6°, which is substantially less than that observed for previous terpy-containing coordination polymer analogues, resulting in a greater molecular polarizability anisotropy. Thus, both of these key structural angles are close to their ideal values to maximize the observed Δn. However, this structure has a β angle of approximately 60°, illustrated in Figure 8b, which shows the point at which the b-axis cuts each phenpy ligand. This substantial value means that the light only experiences a slice of the maximum polarizability anisotropy of the plane of each phenpy unit down this measurement axis.

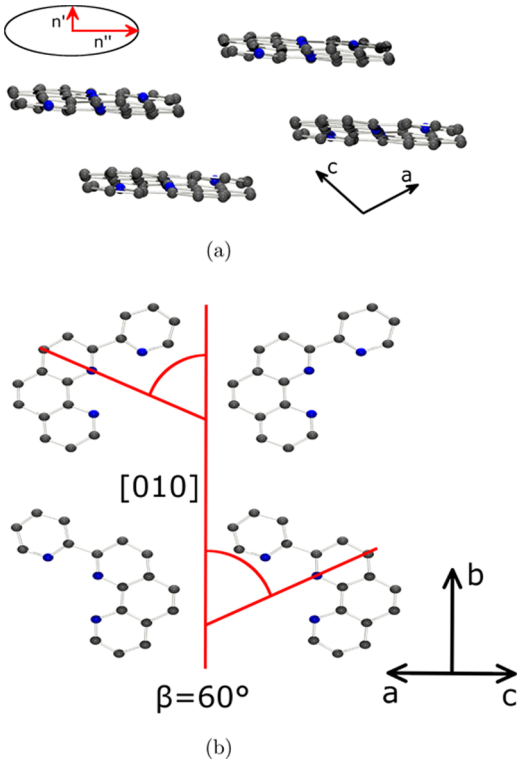

Figure 8. Phenpy packing in the structure of $Cd(phenpy)[Au(CN)_2]_2$. (a) The birefringence measurement view (b-axis) showing only the phenpy units for clarity and an approximate representation of the indicatrix superimposed on this face. (b) A view showing the phenpy plane relative to the birefringence measurement axis. The metals and cyanides units have been removed for clarity. Atom colors: blue, N; gray, C.

In comparison, $Mn(terpy)[Au(CN)_2]_2$ has Δn = 0.388(8) with α = 10.2, β = 3, and γ = 3.5°. These small angles indicate a near ideal orientation of the terpy ligands in this crystal.[16] The Δn of $M(phenpy)[Au(CN)_2]_2$ is identical within experimental error despite phenpy having a higher polarizability anisotropy. Since the α and γ values for the two crystals are quite similar, the much higher β values (60° vs 3°) in $Cd(phenpy)[Au(CN)_2]_2$ likely offset the gains of added polarizability anisotropy of the ligand, resulting in similar Δn values for the two materials.

Birefringence of M(phenpy)(H$_2$O)[Au(CN)$_2$]$_2$·2H$_2$O (M = Mn, Zn, and Cd). The measured birefringence of $Zn(phenpy)(H_2O)[Au(CN)_2]_2{\cdot}2H_2O$ and $Cd(phenpy)(H_2O)[Au(CN)_2]_2{\cdot}2H_2O$ are 0.59(6) and 0.56(3), respectively, and are among the highest Δn values reported for crystalline solids. No measurement of the $Mn(phenpy)(H_2O)[Au(CN)_2]_2{\cdot}2H_2O$ structure could be made due to the poor quality crystals obtained. Figure 9a shows a crystal of $Cd(phenpy)(H_2O)[Au(CN)_2]_2{\cdot}2H_2O$ under crossed polarizers near the point of full compensation with a Berek compensator. The crystals of all

DOI: 10.1021/acs.inorgchem.5b00749
Inorg. Chem. 2015, 54, 6462−6471

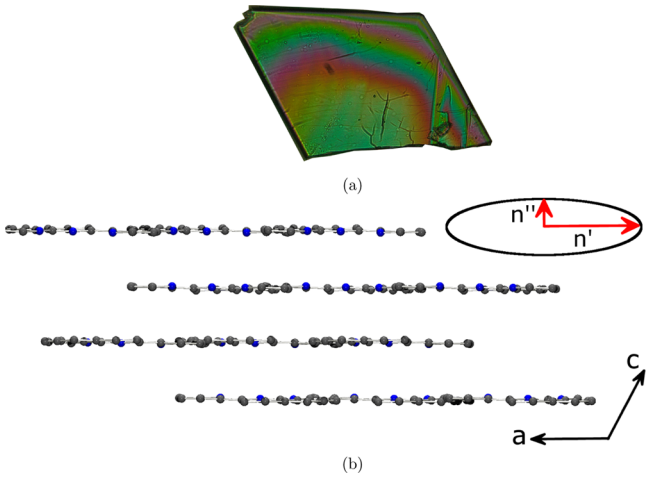

Figure 9. (a) Crystal of Cd(phenpy)(H_2O)[$Au(CN)_2$]$_2$·2H_2O under crossed polarizers near the point of full compensation with a Berek compensator. (b) Phenpy packing in the structure of M(phenpy)-(H_2O)[$Au(CN)_2$]$_2$, looking down the birefringence measurement view (*b*-axis), and an approximate representation of the indicatrix superimposed on this face. Notice the face-to-face alignment of phenpy ligands. The metals, cyanides, and water units have been removed for clarity. Atom colors: blue, N; gray, C.

three M(phenpy)(H_2O)[$Au(CN)_2$]$_2$·2H_2O compounds have plate morphology and are monoclinic. The torsion angle (α) is 1.6°, less than any of the analogous terpy-based derivatives and the aforementioned M(phenpy)[$Au(CN)_2$]$_2$. The primary crystal growth direction is perpendicular to the *b*-axis (Figure 9b), which is oriented almost parallel to the α_y tensor component of phenpy, i.e., β = 6°, and thus light propagating through the material in this direction will experience near maximum polarizability anisotropy of the phenpy units. The γ angle is only 1.5°, and so any decreased polarizability anisotropy from this deviation is negligible. Thus, all three key angles approach the ideal values, accounting for the very large Δn.

In support of this, examining the crystal orientation with respect to the compensator orientation during the Δn measurement reveals that the higher refractive index is indeed along the *a*-axis (Figure 9), consistent with a higher polarizability in this direction (approximately parallel to the α_x tensor component). Therefore, the birefringence is a measure of the difference in refractive index between the in-plane and perpendicular direction of the phenpy ligand (as indicated by the indicatrix projection in Figure 9), and thus, the measured values are likely the maximum possible Δn.

Although comparisons between M(phenpy)(H_2O)[$Au(CN)_2$]$_2$·2H_2O and M(phenpy)[$Au(CN)_2$]$_2$ should only be made with care as the crystals are not isostructural, we can rationalize the differences in Δn values by reference to their β values (Figure 10). Whereas both structures have a small phenpy tilt angle (γ), the M(phenpy)[$Au(CN)_2$]$_2$ structure has a much larger β value (60°) versus that of M(phenpy)(H_2O)-[$Au(CN)_2$]$_2$·2H_2O (6°). The large β value for M(phenpy)-[$Au(CN)_2$]$_2$ indicates that the major contributor to the in-plane refractive index is α_y, which, as already noted, is only two-thirds the magnitude of α_x, leading to a diminished birefringence.

In summary, as hypothesized in the ligand design, extending the π-system increased the anisotropy of the ligand, while still allowing good alignment. Since the M(phenpy)(H_2O)[Au-

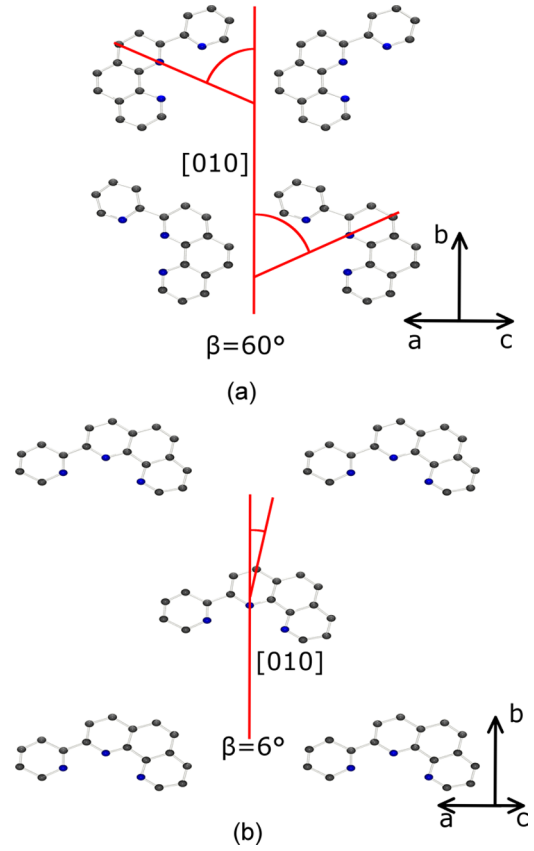

Figure 10. Orientation of phenpy units relative to the birefringence axis for (a) M(phenpy)[$Au(CN)_2$]$_2$ and (b) M(phenpy)(H_2O)[Au-($CN)_2$]$_2$·2H_2O. Only phenpy units shown for clarity. Atom colors: blue, N; gray, C.

($CN)_2$]$_2$·2H_2O materials meet all four design criteria, the resulting Δn values are extremely high.

Birefringence of In(phenpy)(Cl)$_2$[Au(CN)$_2$]·0.5H_2O. The measured birefringence of In(phenpy)(Cl)$_2$[$Au(CN)_2$]·0.5H_2O is 0.50(3). The crystals of In(phenpy)(Cl)$_2$[$Au(CN)_2$]·0.5H_2O have plate morphology and are monoclinic, growing perpendicular to the *b*-axis. A view in this direction (Figure 11a) shows excellent alignment of phenpy units (γ = 1.5°). However, highly polarizable In−Cl bonds are located perpendicular to the plane of the phenpy units, creating a decrease in the overall polarizability anisotropy of the material. On the other hand, the [$Au(CN)_2$]$^-$ units are parallel to the phenpy units (Figure 11b), adding to the overall polarizability anisotropy of the system. This underscores the importance of designing a structure in which the highly anisotropic components are aligned. Figure 11c shows the point at which the *b*-axis cuts each phenpy ligand, yielding a β angle of 41°; i.e., there is an averaging of the α_x and α_y contribution to the in-plane refractive index, which again results in an observed decreased birefringence. Although it is difficult to deconvolute, the combination of these opposing geometric factors likely accounts for most of the difference in the birefringence of the In(phenpy)(Cl)$_2$[$Au(CN)_2$]·0.5H_2O and M(phenpy)(H_2O)-[$Au(CN)_2$]$_2$·2H_2O systems.

Table 1 compiles the birefringence data as well as summarizes the relevant phenpy orientation angles. The α and γ angles are consistently very low for all the materials and thus are already optimized to their ideal values, ensuring that Δn will be high. Because these values are all of similar

DOI: 10.1021/acs.inorgchem.5b00749
Inorg. Chem. 2015, 54, 6462−6471

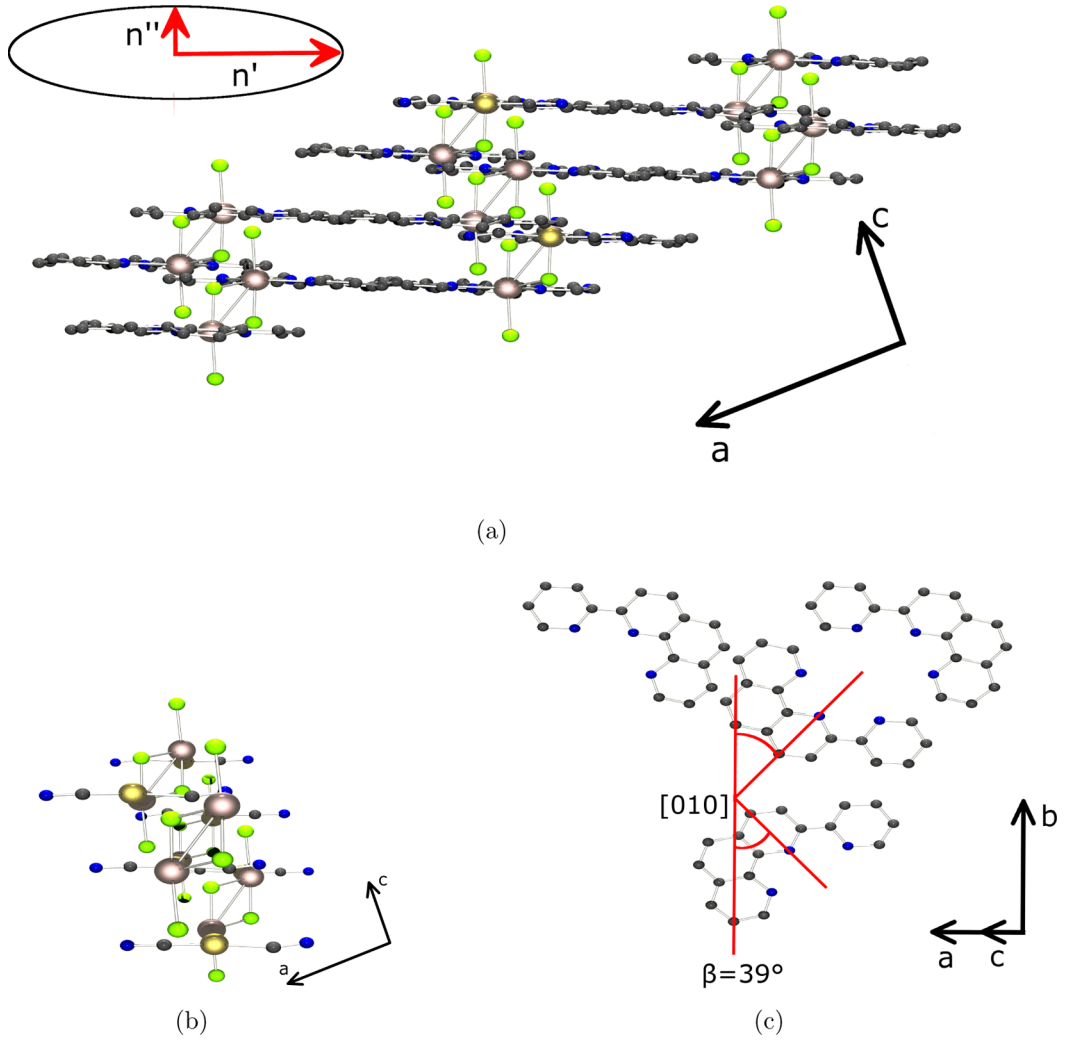

Figure 11. Phenpy packing in the structure of In(phenpy)$(Cl)_2[Au(CN)_2]\cdot 0.5H_2O$. (a) A view down the *b*-axis and an approximate representation of the indicatrix superimposed on this face. Notice the face-to-face alignment of phenpy ligands. The water molecules and $[Au(CN)_2]^-$ units have been removed for clarity. (b) A view down the *b*-axis face showing the alignment of the $[Au(CN)_2]^-$ units perpendicular to the In−Cl bonds. The water molecules and phenpy units have been removed for clarity. (c) A view of the phenpy plane relative to the *b*-axis. The metals, cyanides, chlorides, and water units have been removed for clarity. Atom colors: pink, In; gold, Au; green, Cl; blue, N; gray, C.

Table 1. Data for Structure−Birefringence Analysis

compd ref	α	β	γ	Δn
$Cd(phenpy)[Au(CN)_2]_2$	3.6	60	4.0	0.37(2)
$In(phenpy)(Cl)_2[Au(CN)_2]\cdot 0.5H_2O$	4	41	0	0.50(3)
$Zn(phenpy)(H_2O)[Au(CN)_2]_2\cdot 2H_2O$	1.6	6	1.5	0.59(6)

magnitude, they cannot explain the variations in Δn. However, the β values for each material correlate well in an inverse relationship with Δn; i.e., a higher β value leads to a lower Δn value. In general, simplifying the structures into three angles coupled with the polarizability anisotropy calculation results provides a meaningful comparison where the differences in β values are likely the key significant factor in the differences in Δn values.

In conclusion, an in-depth analysis of the structural differences of six new compounds shows the key design elements that change the overall birefringence. Calculated polarizability tensor components of phenpy show that the magnitudes of differences in α, β, or γ angles (Figure 6) change the overall polarizability anisotropy of the crystals and thus result in a range of Δn values: 0.37(2) ($Cd(phenpy)[Au(CN)_2]_2$), 0.50(3) ($In(phenpy)(Cl)_2[Au(CN)_2]\cdot 0.5H_2O$), 0.56(3) and 0.59(6) ($M(phenpy)(H_2O)[Au(CN)_2]_2\cdot 2H_2O$, M = Cd and Zn, respectively). By focusing only on the building blocks that contribute the most polarizability anisotropy to the structure (in this case, the phenpy molecules), the structural analysis has been simplified, allowing for meaningful comparison of nonisostructural structures. The addition of a carbon−carbon double bond to terpy has increased the polarizability anisotropy of the building block, and as all structures have reduced α and γ angles in comparison to terpy and terpy derivative structures, this makes phenpy more reliable, leading to an increased polarizability anisotropy within the structures and consequently higher Δn values that are among the highest reported for crystalline solids. More importantly, the principles elucidated herein and the associated structural analysis methodology can be harnessed to rationalize the properties of known materials and to design new anisotropic materials for a wide range of optical applications.

DOI: 10.1021/acs.inorgchem.5b00749
Inorg. Chem. 2015, 54, 6462−6471

EXPERIMENTAL SECTION

General Procedures. All reactions were conducted in air. All reagents were obtained from commercial sources and used as received. All hydrothermal reactions were performed in a 5 mL ampule with 3 mL of water, sealed under reduced pressure. The hydrothermal temperature program consisted of a ramping period of 3 h to reach the temperature stated for each compound. This temperature was held for the time stated for each compound, followed by a cool-down period also lasting the time stated for each compound, reaching a final temperature of 25 °C.

IR spectra were recorded on a Thermo Nicolet Nexus 670 FTIR spectrometer equipped with a Pike MIRacle attenuated total reflection (ATR) sampling accessory. Raman spectra were recorded on a Renishaw inVia Raman microscope equipped with a 200 mW 785 nm laser. Spectra were obtained from 100 to 3200 cm^{-1} using a 1200 l/mm (633/780) grating for an exposure time of 10 s. Specific accumulations (*a*) and % laser power (%lp) are stated for each experiment. Microanalyses (C, H, N) were performed by Frank Haftbaradaran and Paul Mulyk at Simon Fraser University on a Carlo Erba EA 1110 CHN elemental analyzer.

Matrix assisted laser desorption ionization time-of-flight mass spectrometry (MALDI-TOF-MS) experiments were determined with a Bruker Autoflex Speed spectrometer (Bruker Daltonics, Bremen, Germany) equipped with a 1 kHz smartbeam-II laser. Positive ion mass spectra were acquired typically within the 300−7000 *m*/*z* range. The mass spectrometer was operated in the reflectron mode, and the mass spectrum obtained for each image position corresponds to the averaged mass spectra of a minimum of 5000 consecutive laser shots. Flex Control 3.4 and flexAnalysis 3.4 software packages (Bruker Daltonics, Bremen, Germany) were used to control the mass spectrometer, set spectrum parameters, and visualize spectral data. Samples were irradiated without a matrix.

Synthesis of 2-(2-Pyridyl)-1,10-phenanthroline. The synthesis of phenpy has previously been reported, and we slightly modified the synthesis as follows.[22] A solution of nBuLi (21 mL, 0.034 mol, 1.6 M solution in hexane) was added to a dry ether (30 mL) solution of 2-bromopyridine (3.2 mL, 0.033 mmol) at −78 °C under N_2. The dark red solution was stirred at −78 °C for 30 min after which it was transferred to a cold (−78 °C), colorless, dry THF solution (60 mL) of 1,10-phenanthroline (5.0 g, 0.028 mol) under N_2. The resulting dark red solution was stirred for 30 min at −78 °C followed for another 2 h at room temperature. Approximately 30 mL of water was added dropwise to the dark red reaction mixture. The reaction mixture turned dark green. The mixture was placed in the fridge overnight after which a pale orange solution remained. The organic solvent was removed in vacuo, and the organics were extracted with CH_2Cl_2. The solution was dried with Na_2SO_4, filtered, and concentrated in vacuo. The crude oil was purified by column chromatography on silica with a 2:1 hexane/Et_2O mixture as the eluent. The solvent was removed in vacuo to yield an orange oil. The crude product was recrystallized by dissolving in minimal methanol (ca. 10 mL) after which a large amount of water was added (ca. 100 mL). A fine powder precipitated immediately. After 8 h the solution was filtered, yielding a pale yellow powder of phenpy. Yield: 2.3 g (28%). Anal. Calcd for $C_{17}H_{15}N_3O_2$: C 69.60%; H 5.15%; N 14.33%. Found: C 69.23%; H 5.08%; N 13.89%. ^1H NMR in $CDCl_3$ (ppm): 9.33 (dd, 1H), 9.14 (d, 1H), 8.86 (d, 1H), 8.75 (d, 1H), 8.41 (d, 1H), 8.37 (dd, 1H), 7.96 (dt, 1H), 7.90 (d, 1H), 7.84 (d, 1H), 7.73 (dd, 1H), 7.39 (dd, 1H).[22]

Synthesis of Zn(phenpy)(H$_2$O)[Au(CN)$_2$]$_2$·2H$_2$O. A pale yellow methanol solution (10 mL) of phenpy (29 mg, 0.10 mmol) was added to an aqueous solution (10 mL) containing $Zn(NO_3)_2·6H_2O$ (30 mg, 0.10 mmol). A methanol/water solution (20 mL, 1:1) of $KAu(CN)_2$ (57 mg, 0.20 mmol) was added to the resulting yellow solution. After 12 h, plate crystals of $Zn(phenpy)(H_2O)[Au(CN)_2]_2·2H_2O$ had formed. The solution was allowed to slowly evaporate for 14 days after which it was filtered. Yield: 68 mg (82%). Anal. Calcd for $C_{21}H_{13}N_7Au_2OZn$: C 30.07%; H 1.56%; N 11.69%. Found: C 30.01%; H 1.64%; N 11.43%. IR (KBr, cm^{-1}) 3429 s, 3067 w, 2192 s, 2180 sh, s, 2153 s, 1581 s, 1505 m, 1500 m, 1470 w, 1427 m, 1326 m, 1254 w, 1233 w, 1202 w, 1166 w, 1147 m, 1130 w, 1035 w, 1011 m, 911 w, 893 w, 852 s, 830 m, 823 w, 776 s, 732 s, 651 s.

Synthesis of Mn(phenpy)(H$_2$O)[Au(CN)$_2$]$_2$·2H$_2$O. A pale yellow methanol solution (10 mL) of phenpy (29 mg, 0.10 mmol) was added to an aqueous solution (10 mL) containing $MnCl_2·4H_2O$ (20 mg, 0.10 mmol). A methanol/water solution (20 mL, 1:1) of $KAu(CN)_2$ (57 mg, 0.20 mmol) was added to the resulting yellow solution. After 12 h, plate crystals of $Mn(phenpy)(H_2O)[Au(CN)_2]_2·2H_2O$ had formed. The solution was allowed to slowly evaporate for 14 days after which it was filtered. Yield: 74 mg (85%). Anal. Calcd for $C_{21}H_{13}N_7Au_2MnO·2H_2O$: C 29.18%; H 1.98%; N 11.34%. Anal. Calcd for $C_{21}H_{13}N_7Au_2MnO·H_2O$: C 29.80%; H 1.79%; N 11.59%. Found: C 30.21%; H 1.81%; N 11.37%. IR (KBr, cm^{-1}) 3227 br, m, 3072 w, 2961 w, 2172 m, 2156 s, 2148 s, 1601 m, 1589 m, 1578 s, 1565 w, 1518 m, 1497 m, 1478 m, 1456 w, 1429 m, 1420 w, 1400 m, 1339 w, 1326 m, 1287 w, 1255 m, 1234 m, 1220 w, 1201 m, 1168 w, 1146 s, 1128 w, 1107 w, 1091 w, 1070 w, 1049 w, 1009 s, 905 w, 889 m, 852 s, 831 m, 823 w, 793 w, 775 w, 771 w, 745 w, 731 s.

Synthesis of Cd(phenpy)(H$_2$O)[Au(CN)$_2$]$_2$·2H$_2$O. A pale yellow methanol solution (10 mL) of phenpy (29 mg, 0.10 mmol) was added to an aqueous solution (10 mL) containing $Cd(NO_3)_2·4H_2O$ (30 mg, 0.10 mmol). A methanol/water solution (20 mL, 1:1) of $KAu(CN)_2$ (57 mg, 0.20 mmol) was added to the resulting yellow solution. After 12 h, plate crystals of $Cd(phenpy)(H_2O)[Au(CN)_2]_2·2H_2O$ had formed. The solution was allowed to slowly evaporate for 14 days after which the product was filtered. Yield: 74 mg (84%). Anal. Calcd for $C_{21}H_{13}N_7Au_2CdO·H_2O$: C 27.91%; H 1.67%; N 10.85%. Found: C 27.71%; H 1.62%; N 10.80%. IR (KBr, cm^{-1}) 3429 m, 3088 w, 3062 w, 3048 w, 3014 w, 2991 w, 2178 w, 2143 s, 2098 w, 1587 m, 1516 m, 1494 m, 1470 m, 1435 w, 1425 m, 1396 m, 1337 w, 1322 m, 1255 w, 1230 w, 1218 m, 1199 m, 1144 m, 1126 m, 1104 w, 1092 w, 1068 w, 1045 w, 1038 w, 1009 m, 903 w, 888 m, 857 s, 834 m, 821 m, 795 w, 778 s, 768 s, 743 w, 732 s, 648 s, 582 m, 418 s.

Synthesis of Mn(phenpy)[Au(CN)$_2$]$_2$. $MnCl_2·4H_2O$ (20 mg, 0.1 mmol), phenpy (29 mg, 0.1 mmol), and $KAu(CN)_2$ (57 mg, 0.2 mmol) were added to a 5 mL ampoule with 3 mL of water, which was then sealed under reduced pressure and heated to 120 °C for 12 h before cooling slowly over 60 h. The resulting solution was filtered under vacuum and washed with methanol to give yellow plate crystals, 44 mg (54%) yield. Anal. Calcd for $C_{21}H_{10}N_7MnAu_2$: C 31.15%; H 1.25%; N 12.12%. Found: C 30.98%; H 1.30%; N 11.80%. IR (ATR, cm^{-1}) 2178 s, 2166 vs, 2151 s, 1619 m, 1601 m, 1587 ms, 1578 s, 1518 m, 1497 m, 1478 m, 1431 m, 1400 m, 1326 w, 1289 vw, 1252 w, 1228 w, 1199 vw, 1148 ms, 1127 m, 1091 m, 1047 w, 1010 m, 886 m, 851 ms, 828 m, 771 s, 732 vs. Raman (785 nm; *a*, 1; %lp, 10; cm^{-1}) 2183 vs, 1602 s, 1568 m, 1516 s, 1477 m, 1458 ms, 1429 m, 1339 m, 1293 s, 1253 w, 1142 vw, 1068 vw, 1039 w, 1008 s, 896 w, 888 w, 770 m, 730 m, 699 w, 581 w, 518 w, 4323 w, 318 m, 265 vw, 211 w, 156 m.

Synthesis of Cd(phenpy)[Au(CN)$_2$]$_2$. $Cd(NO_3)_2·4H_2O$ (30 mg, 0.1 mmol), phenpy (29 mg, 0.1 mmol), and $KAu(CN)_2$ (57 mg, 0.2 mmol) were added to a 5 mL ampoule with 3 mL of water, which was then sealed under reduced pressure and heated to 120 °C for 12 h before cooling slowly over 60 h. The resulting solution was filtered under vacuum and washed with methanol to give yellow plate crystals, 29 mg (33%) yield. Anal. Calcd for $C_{21}H_{10}N_7CdAu_2$: C 29.03%; H 1.16%; N 11.29%. Found: C 29.19%; H 1.31%; N 11.21%. IR (ATR, cm^{-1}) 2185 s, 2163 vs, 1619 m, 1601 m, 1589 ms, 1578 ms, 1567 m, 1539 w, 1516 m, 1497 ms, 1475 m, 1434 m, 1425 m, 1400 m, 1339 w, 1324 m, 1290 w, 1256 m, 1234 m, 1201 w, 1170 w, 1149 ms, 1127 m, 1109 w, 1090 w, 1050 w, 1011 m, 890 m, 850 s, 826 m, 769 s, 731 vs. Raman (785 nm; *a*, 1; %lp, 5; cm^{-1}) 2179 s, 1604 s, 1576 m, 1516 s, 1456 m, 1416 ms, 1341 m, 1290 s, 1219 w, 1036 w, 1010 m, 729 w, 530 w, 427 w, 309 w, 158 m.

Synthesis of In(phenpy)(Cl)$_2$[Au(CN)$_2$]·0.5H$_2$O. A pale yellow methanol solution (10 mL) of phenpy (29 mg, 0.1 mmol) was added to an aqueous solution (10 mL) containing $InCl_2·3H_2O$ (28 mg, 0.1 mmol). A methanol/water solution (20 mL, 1:1) of $KAu(CN)_2$ (84 mg, 0.3 mmol) was added to the resulting solution. The solution was allowed to evaporate over 3 weeks giving yellow plate crystals, 49 mg (69%) yield. Anal. Calcd for $C_{19}H_{11}N_5InCl_2Au$-

DOI: 10.1021/acs.inorgchem.5b00749
Inorg. Chem. 2015, 54, 6462−6471

Table 2. Crystallographic Data

	Cd(phenpy)(H_2O)[$Au(CN)_2$]$_2$·$2H_2O$	Zn(phenpy)(H_2O)[$Au(CN)_2$]$_2$·$2H_2O$	Mn(phenpy)(H_2O)[$Au(CN)_2$]$_2$·$2H_2O$	In(phenpy)$(Cl)_2$[$Au(CN)_2$]·$0.5H_2O$	Cd(phenpy)[$Au(CN)_2$]$_2$	Mn(phenpy)[$Au(CN)_2$]$_2$
chemical formula	$C_{21}H_{17}Au_2CdN_7O_3$	$C_{21}H_{17}Au_2N_7O_3Zn$	$C_{21}H_{17}Au_2MnN_7O_3$	$C_{38}H_{24}Au_2Cl_4In_2N_{10}O$	$C_{21}H_{11}Au_2CdN_7$	$C_{21}H_{11}Au_2MnN_7$
fw (g mol^{-1})	921.75	874.72	864.29	1400.03	867.70	810.24
cryst syst	monoclinic	monoclinic	monoclinic	monoclinic	monoclinic	monoclinic
a (Å)	16.286(8)	16.115(6)	16.332(16)	11.3968(9)	10.162(4)	9.9485(10)
b (Å)	22.363(11)	22.124(8)	22.51(2)	25.703(2)	25.868(9)	25.038(3)
c (Å)	14.805(7)	14.647(5)	14.791(15)	7.1857(5)	9.658(3)	10.0688(10)
α (deg)	90	90	90	90	90	90
β (deg)	113.364(4)	112.951(4)	112.960(11)	99.250(2)	114.964(4)	116.8120(10)
γ (deg)	90	90	90	90	90	90
V ($Å^3$)	4950(4)	4809(3)	5008(8)	2077.6(3)	2301.6(14)	2238.4(4)
T (K)	150(2)	150(2)	150(2)	150(2)	150(2)	150(2)
space group	$C2/c$	$C2/c$	$C2/c$	$P2_1/c$	$P2_1/c$	$P2_1/c$
Z	8	8	8	2	4	4
radiation (Å)	0.710 73	0.710 73	0.710 73	0.710 73	0.7749	0.7749
μ (mm^{-1})	12.714	13.200	12.222	8.438	16.914	16.920
reflns all	19 856	16 919	18 214	13 774	23 421	23 372
reflns unique	4380	4404	3065	2181	4221	4121
R_{int}	0.1008	0.1073	0.3127	0.0985	0.1597	0.0510
R1 [$I_0 \geq 2.50\sigma\ (I_0)$]	0.0664	0.1268	0.1002	0.1892	0.0741	0.0613
wR (F^2)	0.1378	0.2627	0.2432	0.4074	0.1727	0.1601
R1 (all data)	0.1317	0.1613	0.1721	0.1958	0.1746	0.0686
wR (F^2) (all data)	0.1697	0.2817	0.2785	0.4106	0.2138	0.1727
GOF	1.027	1.105	1.033	1.265	1.018	1.251

$(H_2O)_{0.5}$: C 32.55%; H 1.73%; N 9.99%. Found: C 32.48%; H 1.85%; N 10.07%. MALDI MS M^+: 442.206, 424.265. Calcd for In(phenpy)-Cl_2 441.94. Calcd for In(phenpy)Cl(OH) 423.97. IR (ATR, cm^{-1}) 3540 br, s, 3438 br, s, 3077 br, m, 2148 m, 1621 m, 1598 m, 1583 s, 1521 w, 1500 m, 1479 m, 1437 m, 1428 m, 1406 m, 1329 w, 1262 w, 1232 w, 1202 w, 1172 w, 1154 m, 1131 w, 1105 w, 1095 w, 1021 m, 893 m, 858 s, 777 s, 727 vs. Raman (785 nm; *a*, 1; %lp, 10; cm^{-1}) 2163 m, 1607 s, 1567 m, 1521 ms, 1479 m, 1460 m, 1428 m, 1418 m, 1353 m, 1331 m, 1298 s, 1262 w, 1236 vw, 1172 vw, 1111 vw, 1072 vw, 1040 w, 1019 ms, 893 vw, 777 m, 736 m, 640 vw, 585 vw, 519 w, 442 w, 425 w, 308 w, 296 w, 281 w, 260 w, 206 w, 182 w, 140 m, 120 m.

Measurement of Birefringence. The optical retardation and crystal thickness measurements were obtained by means of polarized-light microscopy using an Olympus BX60 microscope, with a tilted U-CTB thick Berek compensator at λ = 546(10) nm at room temperature (Supporting Information Figure S2). Retardation measurements were also conducted at λ = 650(20) nm, resulting in a <1% difference, which is far less than the error associated with thickness measurements. The birefringence was calculated by dividing the measured retardation by the crystal thickness. In the case of all crystals in this Article, face assignment of the crystals was determined using the crystal faces application in APEX II. The relatively large errors in the birefringence values for Zn(phenpy)(H_2O)[$Au(CN)_2$]$_2$·$2H_2O$ and Cd(phenpy)(H_2O)[$Au(CN)_2$]$_2$·$2H_2O$ are due to the inherent error in obtaining thickness measurements on very thin (<10 μm) crystals.

Single Crystal X-ray Diffraction Structure Determinations. Structures Cd(phenpy)[$Au(CN)_2$]$_2$ and Mn(phenpy)[$Au(CN)_2$]$_2$ were collected through the SCrALS (Service Crystallography at Advanced Light Source) program at the Small-Crystal Crystallography Beamline 11.3.1 at the Advanced Light Source (ALS), Lawrence Berkeley National Laboratory. Structures In(phenpy)$(Cl)_2$[$Au(CN)_2$]·$0.5H_2O$ and M(phenpy)(H_2O)[$Au(CN)_2$]$_2$·$2H_2O$ (M = Mn, Zn, and Cd) were covered with Paratone, mounted on a MiTe-Gen sample holder, and rapidly placed into the cold N_2 stream of the Kryo-Flex low-temperature device. The data were collected using a Bruker SMART APEX II Duo CCD diffractometer with TRIUMPH graphite-monochromated Mo Kα radiation (λ = 0.710 73 Å). All structures except Mn(phenpy)[$Au(CN)_2$]$_2$ give poor diffraction patterns despite collection using a synchrotron source, and thus the structural models are of poor quality. Additional crystallographic information can be found in Table 2. All diffraction data were processed with the Bruker Apex II software suite. All structures were solved with intrinsic phasing method,[24] and subsequent refinements were performed using SHELXle.[25] Diagrams were prepared using ORTEP-3[26] and POV-RAY.[27]

In the case of In(phenpy)$(Cl)_2$[$Au(CN)_2$]·$0.5H_2O$ the temperature factor on the bridging chloride (Cl2) is quite large, and modeling this atom as a hydroxide results in a lower *R*-factor. However, both CHN elemental analysis and MALDI mass spectrometry data are consistent with a dichloride species, and therefore, the atom has been assigned as a chloride ligand (slow partial hydrolysis of the crystals over time may be to blame for this). In any case, the assignment of that atom does not affect the conclusions of the Article. The pyridine bridge in the phenpy unit is disordered over two sites; C16 and C17 0.27 occupancy, C18 and C19 0.73 occupancy. Rotax analysis found a nonmerohedral twin by an 180 rotation about the [001] direction in real space.

Calculations. Energy calculation was performed using the Gaussian 09 program,[28] the B3LYP functional,[29] and the 6-31G**basis set with the keyword "Polar" on all atoms. The atom coordinates for phenpy were taken from the structure of Cd(phenpy)-(H_2O)[$Au(CN)_2$]$_2$·$2H_2O$.

■ ASSOCIATED CONTENT

Supporting Information

UV−vis data, optical microscopy images, and crystallographic data in CIF format. The Supporting Information is available free of charge on the ACS Publications website at DOI: 10.1021/acs.inorgchem.5b00749.

DOI: 10.1021/acs.inorgchem.5b00749
Inorg. Chem. 2015, 54, 6462−6471

AUTHOR INFORMATION

Corresponding Authors

*E-mail: vancew@sfu.ca.

*E-mail: dleznoff@sfu.ca.

Present Address

[§]Currently at Memorial University of Newfoundland.

Notes

The authors declare no competing financial interest.

ACKNOWLEDGMENTS

NSERC of Canada is gratefully acknowledged for ongoing support of this research via Discovery Grants (D.B.L., V.E.W.) and a postgraduate fellowship (M.J.K.). We thank Benson Jelier (SFU) for collecting the MALDI mass spectrometry data. The Advanced Light Source (ALS) is supported by the U.S. Department of Energy, Office of Energy Sciences Materials Sciences Division, under Contract DE-AC02-05CH11231.

REFERENCES

(1) Newnham, R. E. *Properties of Materials: Anisotropy, Symmetry, Structure*; Oxford University Press: Oxford, U.K., 2005.

(2) Hecht, E. *Optics*, 4th ed.; Addison Wesley: San Francisco, 2002.

(3) Tilley, R. J. D. *Colour and the Optical Properties of Materials: An Exploration of the Relationship between Light, the Optical Properties of Materials and Colour*, 2nd ed.; Wiley: Chichester, U.K., 2011.

(4) Will, I.; Klemz, G. *Opt. Express* **2008**, *16*, 14922−37.

(5) Bendimerad, D. F.; Benkelfat, B.; Member, S.; Hamdi, R.; Gottesman, Y.; Seddiki, O.; Vinouze, B. *J. Lightwave Technol.* **2012**, *30*, 2103−2109.

(6) Shabtay, G.; Eidinger, E.; Zalevsky, Z.; Mendlovic, D.; Marom, E. *Opt. Express* **2002**, *10*, 1534−1541.

(7) Aeed, S. S.; Os, P. J. B.; Zili, L. I. *Jpn. J. Appl. Phys.* **2001**, *40*, 3266−3271.

(8) Velasquez, P.; del Mar Sanchez-Lopez, M.; Moreno, I.; Puerto, D.; Mateos, F. *Am. J. Phys.* **2005**, *73*, 357.

(9) Fiore, A.; Berger, V.; Rosencher, E.; Bravetti, P.; Nagle, J. *Nature* **1998**, *391*, 463−466.

(10) Zhang, M.; Huo, G. *Opt. Eng.* **2014**, *53*, 086105.

(11) Zabotnov, S. V.; Konorov, S. O.; Golovan, L. A.; Fedotov, A. B.; Zheltikov, A. M.; Timoshenko, V. Y.; Kashkarov, P. K.; Zhang, H. *J. Exp. Theor. Phys.* **2004**, *99*, 28−36.

(12) Kashkarov, P. K.; Golovan, L. A.; Fedotov, A. B.; Efimova, A. I.; Kuznetsova, L. P.; Timoshenko, V. Y.; Sidorov-Biryukov, D. A.; Zheltikov, A. M.; Haus, J. W. *J. Opt. Soc. Am. B* **2002**, *19*, 2273.

(13) Khoo, I. C.; Werner, D. H.; Kwon, D. H.; Diaz, A. *Mol. Cryst. Liq. Cryst.* **2008**, *488*, 88−99.

(14) Vuks, M. F. *Opt. Spectrosc.* **1966**, *20*, 361.

(15) Thompson, J. R.; Ovens, J. S.; Williams, V. E.; Leznoff, D. B. *Chem.—Eur. J.* **2013**, *19*, 16572−8.

(16) Katz, M. J.; Kaluarachchi, H.; Batchelor, R. J.; Bokov, A. A.; Ye, Z.-G.; Leznoff, D. B. *Angew. Chem., Int. Ed.* **2007**, *46*, 8804−7.

(17) Katz, M. J.; Leznoff, D. B. *J. Am. Chem. Soc.* **2009**, *131*, 18435−44.

(18) Thompson, J. R.; Roberts, R. J.; Williams, V. E.; Leznoff, D. B. *CrystEngComm* **2013**, *15*, 9387.

(19) Bowes, K. F.; Clark, I. P.; Cole, J. M.; Gourlay, M.; Griffin, A. M. E.; Mahon, M. F.; Ooi, L.; Parker, A. W.; Raithby, P. R.; Sparkes, H. A.; Towrie, M. *CrystEngComm* **2005**, *7*, 269.

(20) Bessel, C. A.; See, R. F.; Jameson, D. L.; Churchill, R.; Takeuchi, K. J. *J. Chem. Soc., Dalton Trans.* **1992**, 3223−3228.

(21) Weber, M. J. *Handbook of Optical Materials*; CRC Press: Boca Raton, FL, 2003.

(22) Moore, J. J.; Nash, J. J.; Fanwick, P. E.; Mcmillin, D. R. *Inorg. Chem.* **2002**, *41*, 6387−6396.

(23) Katz, M. J.; Aguiar, P. M.; Batchelor, R. J.; Bokov, A. A.; Ye, Z.-G.; Kroeker, S.; Leznoff, D. B. *J. Am. Chem. Soc.* **2006**, *128*, 3669−76.

(24) Sheldrick, G. M. *SHELXT v2014*; Bruker AXS Inc.: Madison, WI.

(25) Hübschle, C. B.; Sheldrick, G. M.; Dittrich, B. *J. Appl. Crystallogr.* **2011**, *44*, 1281−1284.

(26) Farrugia, L. J. *J. Appl. Crystallogr.* **2012**, *45*, 849−854.

(27) Fenn, T. D.; Ringe, D.; Petsko, G. A. *J. Appl. Crystallogr.* **2003**, *36*, 944−947.

(28) Frisch, M. J.; et al. *Gaussian 09*; Gaussian Inc.: Pittsburgh, PA, 2009.

(29) Stephens, P. J.; Devlin, F. J.; Chabalowski, C. F.; Frisch, M. J. *J. Phys. Chem.* **1994**, *98*, 11623−11627.

DOI: 10.1021/acs.inorgchem.5b00749
Inorg. Chem. 2015, 54, 6462−6471